



1 **Evidence of intense climate variation and reduced ENSO**
2 **activity from $\delta^{18}\text{O}$ of *Tridacna* 3700 years ago**

3
4 Yue Hu ^{a,b}, Xiaoming Sun ^{a,b,c,d*}, Hai Cheng ^{e,f}, Hong Yan ^{g,h,i*}

5
6 ^a School of Marine Sciences, Sun Yat-sen University, Guangzhou 510006, China

7 ^b Guangdong Provincial Key Laboratory of Marine Resources and Coastal Engineering,
8 Guangzhou 510275, China

9 ^c School of Earth Sciences and Engineering, Sun Yat-sen University, Guangzhou 510275, China

10 ^d Southern Marine Science and Engineering Guangdong Laboratory (Zhuhai), Zhuhai 519000,
11 China

12 ^e Institute of Global Environmental Change, Xi'an Jiaotong University, Xi'an 710054, China

13 ^f Department of Earth Sciences, University of Minnesota, Minneapolis, Minnesota 55455, USA

14 ^g State Key Laboratory of Loess and Quaternary Geology, Institute of Earth Environment, Chinese
15 Academy of Sciences, Xi'an 710061, China

16 ^h CAS Center for Excellence in Quaternary Science and Global Change, Xi'an 710061, China

17 ⁱ OCCES, Qingdao National Laboratory for Marine Science and Technology, Qingdao 266061,
18 China

19 *Corresponding authors: eessxm@mail.sysu.edu.cn; yanhong@ieecas.cn

20

21 **Abstract**

22 *Tridacna* is the largest marine bivalves in the tropical ocean, and its carbonate shell can shed
23 light on high-resolution paleoclimate reconstruction. In this contribution, $\delta^{18}\text{O}_{\text{shell}}$ was used to
24 estimate the climatic variation in the Xisha Islands of the South China Sea. We first evaluate the
25 sea surface temperature (SST) and sea surface salinity (SSS) influence on modern rehandled
26 monthly (r-monthly) resolution *Tridacna gigas* $\delta^{18}\text{O}_{\text{shell}}$. The obtained results reveal that $\delta^{18}\text{O}_{\text{shell}}$
27 seasonal variation is mainly controlled by SST and appear insensitive to local SSS change. Thus,
28 the $\delta^{18}\text{O}$ of *Tridacna* shells can be roughly used as a proxy of the local SST: a 1 ‰ $\delta^{18}\text{O}_{\text{shell}}$ change



29 is roughly equal to 4.41 °C of SST. R-monthly $\delta^{18}\text{O}$ of a 40-year *Tridacna squamosa* (3673 ± 28
30 BP) from the North Reef of Xisha Islands was analyzed and compared with the modern specimen.
31 The difference between the average $\delta^{18}\text{O}$ of fossil *Tridacna* shell ($\delta^{18}\text{O} = -1.34$ ‰) and modern
32 *Tridacna* specimen ($\delta^{18}\text{O} = -1.15$ ‰) probably implies a warm climate with roughly 0.84°C higher
33 in 3700 years ago. The seasonal variation in 3700 years ago was slightly decreased compared with
34 that suggested by the instrument data, and the switching between warm and cold-seasons was
35 rapid. Higher amplitude in r-monthly and r-annual reconstructed SST anomalies implies an
36 enhanced climate variability in this past warm period. Investigation of the El Niño-Southern
37 Oscillation (ENSO) variation (based on the reconstructed SST series) indicates a reduced ENSO
38 frequency but more extreme El Niño events in 3700 years ago.

39

40 **Key words:** *Tridacna*; $\delta^{18}\text{O}$; South China Sea; Seasonal variation; Climate variation; ENSO
41 activity

42

43 **1 Introduction**

44 Carbonate skeleton of marine organisms, such as corals, foraminifers, mollusks, have been
45 widely used to reconstruct environmental variation (Aharon, 1983; Batenburg et al., 2011; Ourbak
46 et al., 2006; Schöne et al., 2005; Wanamaker et al., 2011; Yoshimura et al., 2016; Yu et al., 2005).
47 Due to their high sensitivity to the surrounding environment and the ability to preserve of
48 high-resolution physicochemical variations in their skeleton, these marine biogenic carbonates can
49 shed light on the past climate dynamics. *Tridacna* species, as the largest bivalves and usually live
50 in tropical coral reefs, have received increasing scientific attention in the recent decades (Pätzold
51 et al., 1991; Watanabe et al., 1999; Watanabe et al., 2004; Elliot et al., 2009; Ayling et al., 2015).
52 This is because these bivalves and their shells have many favorable properties for recording local
53 environmental changes: they have dense and well-preserved aragonite shells, fast growth rates (up
54 to 1 cm/yr) with clear annual growth lines, and with longevity from several decades to a few
55 centuries. These advantages make *Tridacna* an ideal material for high-resolution reconstruction of
56 interannual, seasonal or even sub-seasonal climatic variations.

57 Previous studies indicated that *Tridacna* species precipitate their shells with the oxygen



58 isotopic ($\delta^{18}\text{O}$) equilibrium with seawater (Aharon, 1991; Aharon and Chappell, 1986; Pätzold et
59 al., 1991; Romanek and Grossman, 1989; Watanabe et al., 1999), and the influence of ontogenic
60 reduction on the *Tridacna* $\delta^{18}\text{O}$ is negligible (Welsh et al., 2011). These studies implied that
61 $\delta^{18}\text{O}_{\text{shell}}$ can be used to reconstruct the late Quaternary Sea-level and climatic changes. Indeed,
62 $\delta^{18}\text{O}$ of marine biogenic carbonates are not only influenced by sea surface temperature (SST) but
63 also by surrounding seawater $\delta^{18}\text{O}$. Meanwhile, seawater $\delta^{18}\text{O}$ have a close correlation with sea
64 surface salinity (SSS), which is affected by tropical evaporation and precipitation balance.
65 Nonetheless, the SST and SSS influence on $\delta^{18}\text{O}_{\text{shell}}$ is uncertainties due to the distinct variation of
66 temperature and salinity in different area. For example, $\delta^{18}\text{O}_{\text{shell}}$ of the *Tridacna* from
67 southwestern Japan could be directly used as a proxy of SST (Yamanashi et al., 2016), while
68 $\delta^{18}\text{O}_{\text{shell}}$ of Indonesian *Tridacna* were interpreted to be contributed 71.4 % by SST and 28.6 % by
69 SSS (Arias-Ruiz et al., 2017). Thus, local calibration from modern *Tridacna* is important to
70 determine the relationship of $\delta^{18}\text{O}_{\text{shell}}$, SST and SSS.

71 Climatic variation in the Meghalayan (began at 4200 BP in late Holocene) has significant
72 impacts on human society and ecosystem development. However, the early Meghalayan climatic
73 conditions in SE Asia around the South China Sea still remain poorly understood. Shi (1994)
74 reviewed the data from various sources (like ice core, inland lakes, paleosols in loess and eolian
75 sands, sea level fluctuations, palynological and botanical studies) in China, indicating the early
76 Maghalayan was involved in Holocene Megathermal period (8 to 3 ka BP). Sediments in the
77 South China Sea also implied the temperature may have been relatively higher in the early of
78 Meghalayan than present (Ouyang et al., 2016). However, those studies are low- resolution, the
79 high-resolution records under interannual climate variation are rare. With global warming and
80 many climatic disasters occur nowadays, the climatic conditions in the early Meghalayan could
81 serve as an analogue to the modern problems, and have received increasing scientific attention
82 (Schirrmacher et al., 2019; Scuderi et al., 2019; Toth and Aronson, 2019; Zhang et al., 2018).
83 High-resolution isotopic geochemical data on the *Tridacna* in this period become an insight into
84 the climatic variations, including extreme ones.

85 Furthermore, the El Niño-Southern Oscillation (ENSO) is widely accepted to be a main
86 trigger for interannual climatic variability in the Pacific Ocean. Previous studies suggested that the



87 impacts of ENSO activity would not be limited to the tropical area, but also on the global
88 atmospheric circulation through heating-up of the tropical atmosphere (Cane, 2005). A
89 fragmentary understanding of the ENSO dynamics causes the uncertainties to predict current or
90 future variation. Many published models of ENSO behavior (on the average climate and
91 background of the tropical Pacific) were constructed with low-resolution proxy data (Clement et
92 al., 1999), so it seems seasonal or monthly data are important to examine the precise variation in
93 ENSO activity. Recent studies on the late Holocene ENSO evolution yielded controversial
94 findings: Coral records from the tropical Christmas Island showed a reduced ENSO variability
95 around the late Holocene (McGregor et al., 2013; Woodroffe et al., 2003), yet some other studies
96 indicate strengthening ENSO activity at 4 to 3 ka BP (Tudhope et al., 2001; Duprey et al., 2014;
97 Yang et al., 2019). Thus, this further points to the importance of high-resolution isotopic
98 geochemical data in unraveling the dynamics of ENSO from the local to global scale.

99 This study aims to evaluate the seasonality, climate variation, and ENSO activity in the
100 Xisha Islands of the northern South China Sea, based on two high-resolution $\delta^{18}\text{O}_{\text{shell}}$ profiles of
101 modern and fossil *Tridacna*. The study area situated in the northwest margin of the West Pacific
102 Warm Pool (WPWP), and the local climate is widely accepted to be directly responsive to ENSO
103 activity (Mitsuguchi et al., 2008; Yan et al., 2010). A modern *Tridacna gigas* shell was first to
104 estimate the extent of environmental control (SST and SSS) on $\delta^{18}\text{O}_{\text{shell}}$, and a new SST- $\delta^{18}\text{O}_{\text{shell}}$
105 linear regression was proposed. Subsequently, a 40-year fossil *Tridacna squamosa* was used to
106 reconstruct the seasonality and climatic variation, and the obtained results are compared with the
107 modern species and meteorological observations. Finally, the ENSO activity and extreme El Niño
108 events were discussed, using the re-established SST anomalies.

109

110 **2 Materials and methods**

111 *2.1 Regional setting*

112 The South China Sea is located in the northwest of WPWP (Fig. 1a), and its interannual
113 climate has a close relation to ENSO activities (Mitsuguchi et al., 2008; Yan et al., 2010). The
114 Xisha Islands in the northern South China Sea (300 km south of Hainan Island) is substantially
115 influenced by two contrasting Asian monsoons from opposite directions: The Asian summer



116 monsoon from the southwest and the Asian winter monsoon from the northeast. These two
117 monsoons give distinct seasonal SST to the *Tridacna* from the coral reefs of the Xisha Islands.
118 Our sample (*Tridacna squamosa* A5) was collected in the North Reef (17°05' N, 111°30' E),
119 whilst the modern *Tridacna gigas* sample YX1 (studied previously by Yan (2013)), was acquired
120 from the Yongxing Island (16°50' N, 112°50' E), which is about 90 kilometers away from the
121 North Reef (Fig. 1a).

122 Meteorological observations (atmosphere temperature (AT), SST, SSS, rainfalls) are obtained
123 from the Institute of Meteorology of China in the Xisha Islands since 1958. Due to the minimum
124 number of YX1 in a year is seven, the time-scale of modern *Tridacna* YX1 is rehandling into
125 seven points/yr, which indicates a rehandled month (r-month) represents 1.7 actual month. All
126 meteorological observations and $\delta^{18}\text{O}_{\text{shell}}$ are using this method to rehandle the time-scale. Figure
127 1d shows the r-monthly-average time series of AT, SST, SSS, rainfall and their standard deviations
128 (SD). The mean SST is 27.77 °C, AT show a highly positive correlation with SST ($r=0.98$), but is
129 0.7 °C lower. The SST seasonality is 5.33 °C, with the lowest value and highest value occurring in
130 1st r-month and 4th r-month, respectively. The Xisha Islands are far from the continent river runoff
131 can hardly influence on SSS. SSS change from 33.25 to 33.81 ‰, and the change is mainly
132 dominated by rainfall: higher SSS in dry winter and lower SSS in wet summer (Fig. 1e).

133 The SST data in the North Reef are acquired from NOAA HadISST, a global monthly SST
134 data with a spatial resolution of $1^\circ \times 1^\circ$ (data grid cell of data includes both the North Reef and the
135 Yongxing Island) from 1982 to 2017. Niño 1 + 2 SST are obtained from NOAA monthly data
136 between 1982 to 2017 (<http://www.cpc.ncep.noaa.gov/data/indices/sstoi.indices>).

137 2.2 Shell descriptions and sample preparation

138 The 29 cm long fossil *Tridacna squamosa* A5 was cut from the umbo to the ventral margin
139 along the axis of maximum growth (Fig. 1b). A 5 mm-thick slice reveals three different zones (Fig.
140 1c): the inner layer, outer layer and the hinge. The inner layer is chosen for the analyses because
141 of its clear growth layer and well-preserved shell. Published data also revealed that the inner layer
142 $\delta^{18}\text{O}$ values were unaffected by different growth rates or ontogeny (Welsh et al., 2011), and could
143 better reflect actual $\delta^{18}\text{O}$ than the inner layer or the hinge (Pätzold et al., 1991; Elliot et al., 2009).

144 The ^{14}C AMS test revealed the fossil *Tridacna gigas* age was 3437 ± 28 BP. For the



145 marine-reservoir effect, the conventional radiocarbon age was 3673 ± 28 BP using the
146 Radiocarbon Calibration Program CALIB 7.10 (<http://calib.org>). Both X-ray diffraction (XRD)
147 and laser Raman spectrometers results were aragonite, no other substances were found.

148 2.3 Stable isotopes

149 Stable isotope samples were micromilled perpendicular to the growth layer under the
150 micro-drill automated system (Micro-Drill New Wave Research, Olympus SZ 61) in the Isotope
151 Laboratory of Xi'an Jiaotong University, China. Each sample was performed under 1 mm long,
152 100 μm deep. Four intervals were used according to the growth rates: 100 μm ($n = 1$ to 268), 150
153 μm ($n = 269$ to 481), 200 μm ($n = 482$ to 657), 300 μm ($n = 658$ to 765) respectively from adult to
154 childhood (Fig. 2).

155 $\delta^{18}\text{O}$ of *Tridacna* was analyzed in the Isotope Laboratory of Xi'an Jiaotong University, using
156 the ThermoFinnigan MAT-253 mass spectrometer fitted with a Kiel Carbonate Device IV. All the
157 results were reported in per mil (‰), relative to the Vienna PeeDee Belemnite (VPDB) standard.
158 The international standard TTB₁ were added to the analyses every 10 to 20 samples to check the
159 reproducibility. Duplicate measurements of TTB₁ standards and samples showed a long-term
160 reproducibility (1σ) of less than 0.14 ‰ and 0.05 ‰, respectively.

161 Published data of the modern *Tridacna* gigas shell YX1 were used to investigate the
162 relationship between *Tridacna* $\delta^{18}\text{O}$ and local climate (Yan et al., 2013). YX1 was collected from
163 the Yongxing Island, 120 km ESE of the North Reef (Fig. 1b). Modern *Tridacna* YX1 $\delta^{18}\text{O}$
164 (VPDB) of internal carbonate standard (GBW04405) is of (average) -8.49 ± 0.14 ‰, and the
165 standards and samples have reproducibility (1σ) of better than 0.08 ‰ and 0.06 ‰, respectively.
166 The average $\delta^{18}\text{O}$ (VPDB) TTB₁ (A5) is also of -8.49 ± 0.14 ‰, which would minimize deviation
167 during comparison.

168 2.4 Data processing and analyses

169 PearsonT3 (Version 2.2, January 2017) was used to test the correlation coefficient. Monthly
170 insolation was calculated in 100 years by AnalySeries 2.0.8 (Laskar et al., 2004), which contained
171 the calculated sigmas of conventional radiocarbon age in *Tridacna* (A5) life span. The years of
172 modern insolation range from 1918 to 2017, and the time-scale of *Tridacna* A5 range from 3722 to
173 3623 BP. Statistical analyses were performed with software of Origin 2018 and PAST 3.18. Since



174 the yearly minimum number in $\delta^{18}\text{O}_{\text{YX1}}$ was seven, thus the isotopic records, climatic data and
175 insolation data were rehandled to seven points/yr with the AnalySeries 2.0.8 (Schöne and Fiebig,
176 2009; Wanamaker et al., 2011). This sclerochronologic rehandling would decrease the growth
177 rates deviation.

178

179 **3 Results**

180 *3.1 $\delta^{18}\text{O}_{\text{A5}}$ record*

181 Seasonal cycles are distinct in the $\delta^{18}\text{O}_{\text{A5}}$ profile (Fig. 2), which show the 40 years of which
182 the *Tridacna* had lived. The $\delta^{18}\text{O}_{\text{A5}}$ range from -2.07 to -0.14 ‰ (mean -1.35 ‰, n=765). After
183 rehandling into 7 points/yr, $\delta^{18}\text{O}_{\text{A5}}$ vary from -1.98 to -0.29 ‰ (mean -1.34 ‰, n=281).

184 *3.2 Sclerochronology*

185 From the shell slice section, 40 dark/light couples (each representing one year) can be seen
186 clearly. Higher $\delta^{18}\text{O}_{\text{A5}}$ values lie in the short dark increments (transparent), corresponding to the
187 low temperature and dry seasons. In contrast, lower $\delta^{18}\text{O}_{\text{A5}}$ values lie in the long light increments
188 (opaque), corresponding to the high temperatures and wet seasons (Fig. 3a).

189 Annual growth rates can be calculated with the $\delta^{18}\text{O}_{\text{A5}}$ seasonal cycles and interval distance
190 (Fig. 3b). The results show that growth rates were higher when *Tridacna* A5 was young, reaching
191 5 mm/yr. The growth then slowed down and stabilized to 1-2 mm/yr after the *Tridacna* had grown
192 mature. Furthermore, daily increments are obvious under the microscope (Fig. 3b). In general,
193 *Tridacna* A5 grew faster in warm seasons and slower in cold seasons (Fig. 3b).

194 The SST observation in the Xisha Islands suggested that the 1st r-month corresponds to
195 almost the lowest SST. Thus, the highest $\delta^{18}\text{O}$ of each cycle was chosen to be the beginning of a
196 year. After the data rehandling, the potential deviation in different growth rates can also be
197 reduced.

198

199 **4 Discussion**

200 *4.1 Relation of SST, SSS and $\delta^{18}\text{O}$ of modern *Tridacna**

201 Previous studies demonstrated that *Tridacna* is in isotopic equilibrium with the surrounding
202 seawater (Aharon, 1983; Watanabe et al., 1999), which also holds true for the *Tridacna* in the



203 South China Sea (Yan et al., 2013). Biogenic carbonate $\delta^{18}\text{O}$ values are in linear correlations with
204 the SST and seawater $\delta^{18}\text{O}_{\text{water}}$ (Aharon and Chappell, 1986; Pätzold et al., 1991; Romanek and
205 Grossman, 1989). We adopted the $\delta^{18}\text{O}_{\text{shell}}\text{-SST-}\delta^{18}\text{O}_{\text{water}}$ Eq. (1) of Grossman and Ku (1986),
206 which is widely used in calculations for tropical aragonite mollusk species. Meanwhile, $\delta^{18}\text{O}_{\text{water}}$
207 has a positive relationship to SSS, thus, $\delta^{18}\text{O}_{\text{water}}$ can be estimated with Eq (2) which is established
208 through seawater in the northern South China Sea (Hong et al., 1997). We merged Eq (1) and (2)
209 into $\delta^{18}\text{O}_{\text{shell}}\text{-SST-SSS}$ (Eq (3)), and used two approaches to discuss the extent of SST and SSS
210 influence on $\delta^{18}\text{O}_{\text{YXI}}$ under different time-scale.

$$211 \text{ SST } (^\circ\text{C}) = 21.8 - 4.69 (\delta^{18}\text{O}_{\text{shell}} - \delta^{18}\text{O}_{\text{water}}) \quad (1)$$

$$212 \delta^{18}\text{O}_{\text{water}} (\text{‰}) = 0.23 \times \text{SSS} - 7.58 \quad (2)$$

$$213 \text{ SST } (^\circ\text{C}) = -13.75 - 4.69 \times \delta^{18}\text{O}_{\text{shell}} + 1.08 \times \text{SSS} \quad (3)$$

214 In the first approach (seasonal time-scale), we hypothesized two conditions: one with
215 constant SSS but varying SST, and the other with constant SST but varying SSS. Two $\delta^{18}\text{O}$
216 profiles can be calculated: $\delta^{18}\text{O}_{\text{SST}}$ (under constant SSS) and $\delta^{18}\text{O}_{\text{SSS}}$ (under constant SST) (Fig.
217 4a). R-monthly mean values were used to minimize the influence of extreme events. The $\delta^{18}\text{O}_{\text{YXI}}$,
218 $\delta^{18}\text{O}_{\text{SST}}$, and $\delta^{18}\text{O}_{\text{SSS}}$ values are of -0.57 to -1.52 ‰, -0.48 to -1.58 ‰, -1.07 to -1.19 ‰,
219 respectively. The $\delta^{18}\text{O}_{\text{SSS}}$ variation is only 0.12 ‰, 14 % of the $\delta^{18}\text{O}_{\text{YXI}}$ variation. The correlation
220 between $\delta^{18}\text{O}_{\text{YXI}}$ and $\delta^{18}\text{O}_{\text{SST}}$ is high ($r = 0.91$, $n = 7$; $r = 0.78$, $n = 77$), and the two $\delta^{18}\text{O}$ profiles
221 show the same trend. This indicates that $\delta^{18}\text{O}_{\text{shell}}$ in the Xisha Islands correspond predominantly to
222 the seasonal SST variation.

223 In the second approach (based on Eq (1) and (2)), the calculated $\delta^{18}\text{O}_{\text{predicted}}$ (by using both
224 actual SST and SSS) were used to compare with $\delta^{18}\text{O}_{\text{YXI}}$ (Table S1). The $\delta^{18}\text{O}_{\text{YXI}}$ and $\delta^{18}\text{O}_{\text{predicted}}$
225 profiles have nearly the same mean value (1.15 ‰ and 1.14 ‰, respectively) and indicate a
226 perfect match ($r = 0.81$, $n = 77$). This confirms that the local *Tridacna* precipitates its shell in
227 oxygen isotopic equilibrium. In order to determine whether the SSS variation in different season
228 affect the predicted SST significantly, we use the actual SSS, constant SSS (mean SSS) and
229 $\delta^{18}\text{O}_{\text{YXI}}$ to calculate predicted SST. Two predicted SST values (one calculated with varying SSS
230 and the other with constant SSS) have high similarity ($r = 0.93$) (Fig. 4e), and they correspond to
231 the variation of actual SST. Each of these predicted SST values is well correlated with the actual



232 SST ($r_{\text{vary}} = 0.79$, $r_{\text{constant}} = 0.78$). This means that the SSS has little influence on the seasonal
233 $\delta^{18}\text{O}_{\text{shell}}$ variation. Thus, we can then use $\delta^{18}\text{O}_{\text{shell}}$ to roughly estimate the seasonal local SST
234 variation, and establish a new SST- $\delta^{18}\text{O}_{\text{shell}}$ linear regression: $\text{SST } (^{\circ}\text{C}) = 22.69 - 4.41 \times \delta^{18}\text{O}_{\text{shell}}$
235 (or $\delta^{18}\text{O}_{\text{shell}} (\text{‰}) = -0.136 \times \text{SST} + 2.634$). A 1 ‰ change of $\delta^{18}\text{O}_{\text{shell}}$ is roughly equal to 4.41°C of
236 SST. Yu (2005) summarized the published $\delta^{18}\text{O}$ -SST slopes for the *Porites lutea* coral from
237 different places, and suggested that the slopes range from -0.134 to -0.189, in which our result lies
238 (-0.136). In addition, corals from Hainan Island revealed a good $\delta^{18}\text{O}$ vs. SST correlation with a
239 linear regression slope of -0.137 (Su et al., 2006), very similar to our result. Consequently, it is
240 reliable to use the new linear regression for reconstructing the past SST with the fossil $\delta^{18}\text{O}_{\text{shell}}$.

241 4.2 Indication of seasonal variation in modern *Tridacna*

242 From both $\delta^{18}\text{O}_{\text{YX1}}$ (-0.60 to -1.52 ‰) and $\delta^{18}\text{O}_{\text{predicted}}$ (-0.47 to -1.57 ‰) profiles (Fig. 4b),
243 clear seasonality is shown with the lowest value occurring in the 1st r-month (cold seasons) and
244 the highest value in the 4th r-month (warm seasons). Variance in $\delta^{18}\text{O}_{\text{YX1}}$ seasonality is 0.19 %
245 shorter than $\delta^{18}\text{O}_{\text{predicted}}$, which may be due to the different growth rates and equidistance sampling
246 mode. In each year, the analyzed *Tridacna* grew faster in warmer seasons than in colder seasons,
247 thus, specimens under equidistance sampling mode would have more samples in the warm seasons.
248 Fewer points in the cold seasons would decrease the values and lead to lower $\delta^{18}\text{O}_{\text{shell}}$ in the 1st
249 r-month, but the higher number of points make $\delta^{18}\text{O}_{\text{shell}}$ close to $\delta^{18}\text{O}_{\text{predicted}}$ in the warm seasons
250 (nearly identical in the 4th r-month. Moreover, throughout the life of the analyzed *Tridacna*, the
251 $\delta^{18}\text{O}_{\text{shell}}$ amplitude is more approached to the actual $\delta^{18}\text{O}_{\text{predicted}}$ under higher number of points
252 (high growth rates) before it reached maturity. After the *Tridacna* reach maturity, the fewer points
253 taken in a year yielded a lower amplitude. This can explain the minor discrepancy between
254 $\delta^{18}\text{O}_{\text{shell}}$ and $\delta^{18}\text{O}_{\text{predicted}}$. As a result, $\delta^{18}\text{O}_{\text{shell}}$ would slightly reduce the actual seasonal variation.
255 However, the correlation between them is high ($r = 0.81$, $n = 77$), and the mean of $\delta^{18}\text{O}_{\text{YX1}}$
256 (-1.15 ‰) and $\delta^{18}\text{O}_{\text{predicted}}$ (-1.14 ‰) values are similar. Therefore, $\delta^{18}\text{O}_{\text{shell}}$ can also be used to
257 estimate the actual seasonal variation, with caution to the slightly reduced variation.

258 4.3 Reconstructed climate with fossil *Tridacna* A5 $\delta^{18}\text{O}$ evidence

259 The fossil *Tridacna* lived in 3700 years ago during the early Meghalayan. The 40 $\delta^{18}\text{O}_{\text{A5}}$
260 cycles reveal that *Tridacna* A5 had probably lived for at least 40 years. After calculating data into



261 r-monthly average profiles, the extreme seasonal variation effects were minimized. The mean
262 $\delta^{18}\text{O}_{\text{A5}}$ profiles is -1.34‰ , with the minimum and maximum of -1.66 and 0.66‰ , respectively
263 (Fig. 4c). Contrasting to the mean value of YX1 (-1.15‰), the lower $\delta^{18}\text{O}_{\text{A5}}$ mean value may have
264 reflected the higher temperature in which the *Tridacna* had lived. To translate into SST (without
265 considering the SSS changes), the temperature was estimated to be roughly 0.84°C higher than
266 present. This agrees with other lines of evidence that suggested a higher temperature during that
267 period (Ouyang et al., 2016), which was considered to be a Holocene Megathermal in China (8.5
268 to 3 ka BP) (Shi et al., 1992).

269 The average r-monthly seasonal range of this period (1‰) is similar to that yielded from
270 YX1 (0.92‰). The standard deviations of $\delta^{18}\text{O}_{\text{A5}}$ (0.38‰ , $n=281$) and $\delta^{18}\text{O}_{\text{YX1}}$ (0.35‰ , $n=77$)
271 also have similarity. These results show similar climate change in 3700 years ago and nowadays.
272 The life of *Tridacna* YX1 (11 years) is much shorter than the fossil *Tridacna* (which lived for at
273 least 40 years), thus, modern observation data were used to do the climatic comparison. After
274 translating $\delta^{18}\text{O}_{\text{A5}}$ into SST (Fig. 5), the reconstructed SST have an average maximum and
275 minimum of 30°C and 25.61°C , respectively, with seasonal variation of 4.39°C . Comparatively,
276 the r-monthly average range of modern observation is 29.33 to 23.99°C (year from 1982 to 2017),
277 with seasonal variation of 5.34°C . The warmer climate in the past indicates that the seasonality
278 variance is about 0.95°C lower. Considering the seasonality discrepancy between $\delta^{18}\text{O}_{\text{shell}}$ and
279 $\delta^{18}\text{O}_{\text{predicted}}$, the $\delta^{18}\text{O}_{\text{shell}}$ has 19% lower seasonal variation than $\delta^{18}\text{O}_{\text{predicted}}$. Therefore, the actual
280 seasonal variation of A5 (roughly 5.23°C) is still below the present seasonality.

281 In addition, the discrepancy between mean $\delta^{18}\text{O}_{\text{A5}}$ and $\delta^{18}\text{O}_{\text{YX1}}$ is 0.19‰ , the lower mean
282 $\delta^{18}\text{O}_{\text{A5}}$ is because of more r-months in lower values. This reveals a possible prolonged high
283 temperature period: Warm seasons may have been longer, while cold seasons are shorter. From the
284 r-monthly insolation comparison between 3700 years ago (3722 to 3623 BP) and recent decades
285 (1918 to 2017) (Fig. 4d), this coincides with the phenomenon that more insolation occurs from the
286 2nd to 5th r-month (warm seasons), yet less insolation occurs in the rest of the year. Due to the
287 more samples in *Tridacna* obtained in the warm seasons, the prolonged high temperature period
288 would be magnified (from the 2nd to 6th r-month) (Fig. 4c). Moreover, compared to the deviation
289 between the total average and r-monthly values, cold seasons have larger deviation and slope. This



290 illustrates a fast switching between cold and warm seasons in 3700 years ago. As $\delta^{18}\text{O}_{\text{predicted}}$ has
291 stronger seasonal variation than $\delta^{18}\text{O}_{\text{shell}}$, the slope should be sharper, means more significant
292 actual seasonal switching.

293 Overall, the climate in around 3700 years ago had slightly lower seasonality than present,
294 and the switching between cold to warm seasons was more serious.

295 *4.4 Climate variation comparison between 3700 years ago and present*

296 Global warming is considered to have triggered many disasters (Burgess et al., 2018;
297 Oppenheimer, 2008; Wang et al., 2015; R. Yu et al., 2018). Analogous studies on past warm
298 climate would allow us to better predict the future climate and extreme events if global warming
299 persists. Therefore, we compared modern instrumental observations (year from 1982 to 2017) in
300 the North Reef with the reconstructed SST anomalies of *Tridacna* A5. R-monthly resolution data
301 were first compared, which were obtained by subtracting the r-monthly SST with the mean value
302 of each r-monthly. In terms of long-term climatic variation, the SST anomalies are markedly
303 different between the 36-year modern instrument data and the 40-year reconstructed data (Fig. 6a).
304 The SST anomalies (3700 years ago) have sharper peaks and higher amplitude than in those of the
305 recent years, and the standard deviation in the past is much larger (0.68 °C) than the present
306 (0.42 °C), which suggest a more severe climate condition in the past. However, one has to be
307 aware of the different growth rates and equidistant sampling mode in *Tridacna*'s life when using
308 the r-monthly resolution. For example, *Tridacna* may have different annual growth rates, hence a
309 r-monthly value may not represent the corresponding actual r-monthly value under equidistant
310 sampling mode. In this respect, the r-annual SST anomalies are estimated (Fig. 6b). The SD of
311 modern observation is 0.30 °C, and the SD of reconstructed SST anomalies is 0.41 °C. This
312 illustrates that the ratios of the modern to the past in r-monthly resolution or r-annual resolution
313 are almost the same (0.65 and 0.73, respectively), thus the SD of r-monthly SST anomalies of
314 *Tridacna* is likely reliable. As a result, there was probably an enhanced climate variability 3700
315 years ago.

316 *4.5 ENSO activity recorded by Tridacna $\delta^{18}\text{O}$*

317 ENSO is the strongest signal in global interannual climate variation, and understanding its
318 mechanism is important to unravel the past climate change and forecast in the future one.



319 Interannual climate changes in the Xisha Islands were likely dominated by ENSO activity, and the
320 local SST anomalies may have reflected 76.47 % and 79.41 % on moderate El Niño and La Niña
321 events, respectively (Liu et al., 2016). Previous studies demonstrated that the marine biogenic
322 carbonate-based SST reconstructions in the northern South China Sea likely responded to ENSO
323 activity (Sun et al., 2005; Yan et al., 2017). Warm/cold SST anomalies were related to El Niño/La
324 Niña events. Coral is one of the earliest records for ENSO events (Peng et al., 2003; Sun et al.,
325 2005; Wei et al., 2007), yet there are still some technical limitations, such as those concerning the
326 calcite-affected data (McGregor and Gagan, 2003). Analyses on the *Tridacna* species were later
327 introduced to make up this imperfection, due to their denser shells, negligible diagenetic alteration,
328 and oxygen isotopic equilibrium with seawater. Recently, Yan et al. (2014) proved that *Tridacna*
329 species in the Xisha Islands could respond to ENSO activity, and then used fossil *Tridacna* $\delta^{18}\text{O}$ in
330 Dongdao Island (one of the islands in the Xisha Islands) to reconstruct ENSO variability around
331 2000 years ago (Yan et al., 2017).

332 To acquire more precise ENSO reconstructions, modern observation data were analyzed. The
333 SST of Niño 1 + 2 region was chosen due to the distinct seasonal variation as the same as the
334 study area, and the SST anomaly series were calculated by subtracting the r-monthly mean values
335 (seven points/yr). The spectral analyses were performed to test periodicity among all SST
336 anomalies (Fig. 7), which indicate spectral peak of three to seven years. According to the SST
337 series, the North Reef SST have a 3-month time lag behind the Niño 1 + 2 SST (Fig. 8a), and thus
338 we bring 3-month forward to eliminate the lag. To reconstruct the occurrence of ENSO-type in the
339 North Reef, 3-7 years bandpass filtering was performed on the SST anomalies, which yielded a
340 tendency of the North Reef ENSO activity mostly consistent with the Niño 1 + 2 SST anomalies
341 (Fig. 8c). We calculated a threshold value under 1σ SST anomalies for moderate El Niño/La Niña
342 events. A total of seven El Niño and ten La Niña events occurred in the past 36 years. In other
343 words, El Niño/La Niña events occurred successively in a 5.14-year frequency in the North Reef.

344 Spectral analysis revealed that $\delta^{18}\text{O}_{\text{A}_5}$ anomalies also have a 3-7 years period (Fig. 7c). As
345 above discussed, the *Tridacna* $\delta^{18}\text{O}$ values are mainly dominated by SST in the Xisha Islands, and
346 1‰ $\delta^{18}\text{O}_{\text{shell}}$ is roughly equal to 4.41 °C of SST. We translate the $\delta^{18}\text{O}_{\text{A}_5}$ anomalies into the North
347 Reef SST_{A₅} anomalies (Fig. 9b). After the 3-7 years bandpass filtering of the North Reef SST_{A₅}



348 anomalies, six El Niño and five La Niña events were estimated to occur in 40 years with 1σ SST_{A5}
349 anomalies threshold (Fig. 9c), giving 6.67-year and 8-year frequency, respectively. The ENSO
350 frequency reduces when comparing with the modern observation data. The lower frequency
351 supported the ENSO reconstructions since 7 ka BP, which suggests a notable reduction of ENSO
352 between 5 ka BP and 3 ka BP (Liu et al., 2013; McGregor et al., 2013; Tudhope et al., 2001;
353 Emile-Geay et al., 2016). However, implications drawn from merely 40-year long *Tridacna* $\delta^{18}\text{O}$
354 record is likely inconclusive. Collection of more similar-age *Tridacna* is needed to acquire a more
355 continuous climate and ENSO activity record.

356 4.6 Extreme winter El Niño records in fossil *Tridacna* $\delta^{18}\text{O}$ values

357 Extreme El Niño brings about many climatic disasters, such as catastrophic flooding,
358 bushfire and drought, in recent decades (Ramírez and Briones, 2017; Staupe-Delgado et al., 2018;
359 Yu et al., 2018; Yu et al., 2019). With global warming persists, the question of whether high
360 temperatures are related to extreme El Niño events is still controversial. Therefore, records of
361 extreme El Niño events in the past warm periods are important. Here, the winter SST is used to
362 estimate the extreme El Niño events. Winters in the northern South China Sea are very dry, and
363 the SSS variation caused by rainfall is small. Thus, the SST determined from $\delta^{18}\text{O}$ should be close
364 to the actual value. The SST calculated by $\delta^{18}\text{O}_{\text{YX1}}$ reveal warmer winter in 1998, corresponding
365 to a stronger El Niño that year. Comparison between the reconstructed SST (calculated with
366 $\delta^{18}\text{O}_{\text{A5}}$) and modern observation data from the North Reef (Fig. 5), suggested that the average
367 winter SST in 3700 years ago was 25.62 °C. There are six distinctly high SST within the 40 years,
368 with the anomalies range from 0.73 to 2.00 °C. As for the SST of modern observation (year from
369 1982 to 2017), the average of winter SST is 23.99 °C, and three anomalously warm temperatures
370 vary from 0.6 to 1.38 °C. It seems that the extreme El Niño events occurred under higher
371 temperature and were more frequent in this past warm period. However, we still have low
372 confidence in answering this controversial question about the relationship between El Niño events
373 and warm climate, more *Tridacna* in the past warm period should be analyzed in future work.
374 Nevertheless, our results still put forward a high-resolution data that make a contribution to future
375 work on how El Niño performs in the warm period.

376



377 5 Conclusions

378 The $\delta^{18}\text{O}$ derived from *Tridacna* provide high-resolution data to unravel the climatic
379 variability and ENSO activity. In the Xisha Islands of northern South China Sea, $\delta^{18}\text{O}_{\text{shell}}$ of
380 modern *Tridacna gigas* can serve as a proxy of SST, while SSS has a minor effect on $\delta^{18}\text{O}_{\text{shell}}$.
381 Thus, a $\delta^{18}\text{O}$ -SST linear regression is established roughly: $\text{SST } (^{\circ}\text{C}) = 22.69 - 4.41 \times \delta^{18}\text{O}_{\text{shell}}$.
382 Another *Tridacna squamosa* A5, which lived 3700 years ago, reveals 40 clearly dark/light couples
383 consistent with $\delta^{18}\text{O}$ amplitude. Reconstructed SST implies a warmer climate in 3700 years ago,
384 0.84 $^{\circ}\text{C}$ higher than present. The seasonal variation slightly decreased and the switching among
385 warm and cold seasons was faster. The combination of r-monthly-/r-annual-resolution
386 reconstructed SST anomalies suggest an enhanced climatic variability during this past warm
387 period. Besides, the frequency of ENSO activity reduced in 3700 years ago than that in recent
388 36-year modern observation. El Niño/La Niña events occurred alternatively in every 6.67-/8-year
389 frequency in the past, compared to 5.14-year nowadays. The extreme winter El Niño has been
390 recorded by fossil *Tridacna* under an increased and intense situation. Our results imply an unstable
391 climate in 3700 years ago, although more data are still needed to support this hypothesis.

392 Author Contributions

393 X. M. S., H. Y., Y. H. designed the research and experiments; H. Y. collected the samples; H.
394 C., Y. H. performed stable isotope measurements. H. Y. and Y. H. did the data analyses. Y. H.
395 wrote the manuscript, with the help of all co-authors.

396 Competing interests

397 The authors declare that they have no conflict of interest.

398 Data and materials availability

399 All data needed to evaluate the conclusions in the paper are presented in the paper. Additional
400 data related to this paper may be requested from the authors. Correspondence and requests for
401 materials should be addressed to X. M. S. (eessxm@mail.sysu.edu.cn) and H. Y.
402 (yanhong@ieecas.cn).

403 Acknowledgments

404 This work is supported by the projects from the National 13th Five Year Plan Project
405 (DY135-R2-1-01, DY135-C1-1-06), National Nature Science Foundation of China (41877399,



406 41876038, 91128101, 41888101), State Key Laboratory for Mineral Deposits Research in Nanjing
407 University (No. 20–15–07), Chinese Academy of Sciences (QYZDB-SSW-DQC001), Qingdao
408 National Laboratory for Marine Science and Technology of China (QNL2016ORP0202), and.
409 We are grateful to Dr. Yu Fu, Dr. Yang Lu, Dr. Jiaoyang Ruan, Chengcheng Liu, Tianjian Yang,
410 Jun Gu for their support in preparing the manuscript. Dr. Youfeng Ning, Hanying Li, Pengfei Duan,
411 Jingyao Zhao are thanked for their technical support in drilling and analyses in Xi’an Jiaotong
412 University.

413 References

- 414 Aharon, P.: 140,000-yr isotope climatic record from raised coral reefs in New Guinea, *Nature*,
415 304(5928), 720–723, <https://doi.org/10.1038/304720a0>, 1983.
- 416 Aharon, P.: Recorders of reef environment histories: stable isotopes in corals, giant clams, and
417 calcareous algae, *Coral Reefs*, 10(2), 71–90, <https://doi.org/10.1007/BF00571826>, 1991.
- 418 Aharon, P. and Chappell, J.: Oxygen isotopes, sea level changes and the temperature history of a
419 coral reef environment in New Guinea over the last 105 years, *Palaeogeogr. Palaeoclimatol.*
420 *Palaeoecol.*, 56(3–4), 337–379, [https://doi.org/10.1016/0031-0182\(86\)90101-X](https://doi.org/10.1016/0031-0182(86)90101-X), 1986.
- 421 Arias-Ruiz, C., Elliot, M., Bézou, A., Pedoja, K., Husson, L., Cahyarini, S. Y., Cariou, E., Michel,
422 E., La, C. and Manssouri, F.: Geochemical fingerprints of climate variation and the extreme
423 La Niña 2010–11 as recorded in a *Tridacna squamosa* shell from Sulawesi, Indonesia,
424 *Palaeogeogr. Palaeoclimatol. Palaeoecol.*, 487, 216–228,
425 <https://doi.org/10.1016/j.palaeo.2017.08.037>, 2017.
- 426 Ayling, B. F., Chappell, J., Gagan, M. K. and McCulloch, M. T.: ENSO variability during MIS 11
427 (424–374 ka) from *Tridacna gigas* at Huon Peninsula, Papua New Guinea, *Earth Planet. Sci.*
428 *Lett.*, 431, 236–246, <https://doi.org/10.1016/j.epsl.2015.09.037>, 2015.
- 429 Batenburg, S. J., Reichert, G. J., Jilbert, T., Janse, M., Wesselingh, F. P. and Renema, W.:
430 Interannual climate variability in the Miocene: High resolution trace element and stable
431 isotope ratios in giant clams, *Palaeogeogr. Palaeoclimatol. Palaeoecol.*, 306(1–2), 75–81,
432 <https://doi.org/10.1016/j.palaeo.2011.03.031>, 2011.
- 433 Burgess, C. P., Taylor, M. A., Spencer, N., Jones, J. and Stephenson, T. S.: Estimating damages
434 from climate-related natural disasters for the Caribbean at 1.5 °C and 2 °C global warming
435 above preindustrial levels, *Reg. Environ. Chang.*, 18(8), 2297–2312,
436 <https://doi.org/10.1007/s10113-018-1423-6>, 2018.
- 437 Cane, M. A.: The evolution of El Niño, past and future, *Earth Planet. Sci. Lett.*, 230(3–4), 227–
438 240, <https://doi.org/10.1016/j.epsl.2004.12.003>, 2005.
- 439 Clement, A. C., Seager, R. and Cane, M. A.: Suppression of El Niño during the mid-Holocene by
440 changes in the Earth’s orbit, *Paleoceanography*, 15(6), 731–737,
441 <https://doi.org/10.1029/1999PA000466>, 2000.
- 442 Duprey, N., Galipaud, J. C., Cabioch, G. and Lazareth, C. E.: Isotopic records from archeological
443 giant clams reveal a variable climate during the southwestern Pacific colonization ca. 3.0ka
444 BP, *Palaeogeogr. Palaeoclimatol. Palaeoecol.*, 404, 97–108,



- 445 <https://doi.org/10.1016/j.palaeo.2014.04.002>, 2014.
- 446 Elliot, M., Welsh, K., Chilcott, C., McCulloch, M., Chappell, J. and Ayling, B.: Profiles of trace
447 elements and stable isotopes derived from giant long-lived *Tridacna gigas* bivalves:
448 Potential applications in paleoclimate studies, *Palaeogeogr. Palaeoclimatol. Palaeoecol.*,
449 280(1–2), 132–142, <https://doi.org/10.1016/j.palaeo.2009.06.007>, 2009.
- 450 Emile-Geay, J., Cobb, K. M., Carre, M., Braconnot, P., Leloup, J., Zhou, Y., Harrison, S. P.,
451 Corrège, T., McGregor, H. V., Collins, M., Driscoll, R., Elliot, M., Schneider, B. and
452 Tudhope, A.: Links between tropical Pacific seasonal, interannual and orbital variability
453 during the Holocene, *Nat. Geosci.*, 9(2), 168–173, <https://doi.org/10.1038/ngeo2608>, 2016.
- 454 Grossman, E. L. and Ku, T. L.: Oxygen and carbon isotope fractionation in biogenic aragonite:
455 Temperature effects, *Chem. Geol.*, 59, 59–74, <https://doi.org/10.1109/TEM.2017.2764526>,
456 1986.
- 457 Hong, A., Hong, Y., Wang, Q. and Ke, J.: Distributive characteristics of O isotope of the
458 northeastern South China Sea in the summer of 1994, *Trop. Oceanol.*, 16(2), 82–90, 1997.
- 459 Laskar, J., Robutel, P., Joutel, F., Gastineau, M., Correia, A. C. M. and Levrard, B.: A long-term
460 numerical solution for the insolation quantities of the Earth, *Astron. Astrophys.*, 428(1),
461 261–285, <https://doi.org/10.1051/0004-6361:20041335>, 2004.
- 462 Liu, C., Zhang, W. and Yan, H.: Relationship between El Niño-Southern Oscillation events and
463 regional sea surface temperature anomalies around the Xisha Islands, South China Sea, *J.*
464 *Pers. Soc. Psychol.*, 1(1), 1188–1197, <https://doi.org/10.1111/j.1469-7610.2010.02280.x>,
465 2016.
- 466 Liu, J., Li, T., Xiang, R., Chen, M., Yan, W., Chen, Z. and Liu, F.: Influence of the Kuroshio
467 Current intrusion on Holocene environmental transformation in the South China Sea,
468 *Holocene*, 23(6), 850–859, <https://doi.org/10.1177/0959683612474481>, 2013.
- 469 McGregor, H. V. and Gagan, M. K.: Diagenesis and geochemistry of Porites corals from Papua
470 New Guinea: Implications for paleoclimate reconstruction, *Geochim. Cosmochim. Acta*,
471 67(12), 2147–2156, https://doi.org/10.1007/430_2015_174, 2003.
- 472 McGregor, H. V., Fischer, M. J., Gagan, M. K., Fink, D., Phipps, S. J., Wong, H. and Woodroffe, C.
473 D.: A weak El Niño/Southern Oscillation with delayed seasonal growth around 4,300 years
474 ago, *Nat. Geosci.*, 6(11), 949–953, <https://doi.org/10.1038/ngeo1936>, 2013.
- 475 Mitsuguchi, T., Dang, P. X., Kitagawa, H., Uchida, T. and Shibata, Y.: Coral Sr/Ca and Mg/Ca
476 records in Con Dao Island off the Mekong Delta: Assessment of their potential for
477 monitoring ENSO and East Asian monsoon, *Glob. Planet. Change*, 63(4), 341–352,
478 <https://doi.org/10.1016/j.gloplacha.2008.08.002>, 2008.
- 479 Oppenheimer, M.: A Physical Science Perspective on Disaster : Through the Prism of Global
480 Warming, *Soc. Res. (New York)*, 75(3), 659–669 [online] Available from:
481 <https://www.jstor.org/stable/40972083>, 2008.
- 482 Ourbak, T., Corrège, T., Malaizé, B., Le Cornec, F., Charlier, K. and Peypouquet, J. P.: ENSO and
483 interdecadal climate variability over the last century documented by geochemical records of
484 two coral cores from the South West Pacific, *Adv. Geosci.*, 6, 23–27,
485 <https://doi.org/10.5194/adgeo-6-23-2006>, 2006.
- 486 Ouyang, T., Li, M., Zhao, X., Zhu, Z., Tian, C., Qiu, Y., Peng, X. and Hu, Q.: Sensitivity of
487 Sediment Magnetic Records to Climate Change during Holocene for the Northern South
488 China Sea, *Front. Earth Sci.*, 4(May), 1–12, <https://doi.org/10.3389/feart.2016.00054>, 2016.



- 489 Pätzold, J., Heinrichs, J. P., Wolschendorf, K. and Wefer, G.: Correlation of stable oxygen isotope
490 temperature record with light attenuation profiles in reef-dwelling *Tridacna* shells, *Coral*
491 *Reefs*, 10(2), 65–69, <https://doi.org/10.1007/BF00571825>, 1991.
- 492 Peng, Z., Chen, T., Nie, B., Head, M. J., He, X. and Zhou, W.: Coral $\delta^{18}\text{O}$ records as an indicator
493 of winter monsoon intensity in the South China Sea, *Quat. Res.*, 59(3), 258–292,
494 [https://doi.org/10.1016/S0033-5894\(03\)00042-5](https://doi.org/10.1016/S0033-5894(03)00042-5), 2003.
- 495 Ramírez, I. J. and Briones, F.: Understanding the El Niño Costero of 2017: The Definition
496 Problem and Challenges of Climate Forecasting and Disaster Responses, *Int. J. Disaster Risk*
497 *Sci.*, 8(4), 489–492, <https://doi.org/10.1007/s13753-017-0151-8>, 2017.
- 498 Romanek, C. S. and Grossman, E. L.: Stable Isotope Profiles of *Tridacna* maxima as
499 Environmental Indicators Stable Isotope Profiles of *Tridacna* maxima as Environmental
500 Indicators, *Palaios*, 4(5), 402–413, <https://doi.org/10.2307/3514585>, 1989.
- 501 Schirrmacher, J., Weinelt, M., Blanz, T., Andersen, N., Salgueiro, E. and Schneider, R. R.:
502 Multi-decadal climate variability in southern Iberia during the mid- to late-Holocene, *Clim.*
503 *Past*, 15(2), 617–634, <https://doi.org/10.5194/cp-15-367-2019>, 2019.
- 504 Schöne, B. R. and Fiebig, J.: Seasonality in the North Sea during the Allerød and Late Medieval
505 Climate Optimum using bivalve sclerochronology, *Int. J. Earth Sci.*, 98(1), 83–98,
506 <https://doi.org/10.1007/s00531-008-0363-7>, 2009.
- 507 Schöne, B. R., Fiebig, J., Pfeiffer, M., Gleß, R., Hickson, J., Johnson, A. L. A., Dreyer, W. and
508 Oschmann, W.: Climate records from a bivalved Methuselah (*Arctica islandica*, Mollusca;
509 Iceland), *Palaeogeogr. Palaeoclimatol. Palaeoecol.*, 228(1–2), 130–148,
510 <https://doi.org/10.1016/j.palaeo.2005.03.049>, 2005.
- 511 Scuderi, L. A., Yang, X., Ascoli, S. E. and Li, H.: The 4.2 ka BP Event in northeastern China : a
512 geospatial perspective, *Clim. Past*, 15(1), 367–375, <https://doi.org/10.5194/cp-15-367-2019>,
513 2019.
- 514 Shi, Y., Kong, Z., Wang, S., Tang, L., Wang, F., Yao, T., Zhao, X., Zhang, P. and Shi, S.: The
515 Climatic Fluctuation and Important Events of Holocene Megathermal in China, *Sci. CHINA*,
516 37(3), 353–365, available from: <http://ir.nigpas.ac.cn/handle/332004/4853>, 1994.
- 517 Staupe-Delgado, R., Kruke, B. I., Ross, R. J. and Glantz, M. H.: Preparedness for slow-onset
518 environmental disasters: Drawing lessons from three decades of El Niño impacts, *Sustain.*
519 *Dev.*, 26(6), 553–563, <https://doi.org/10.1002/sd.1719>, 2018.
- 520 Su, R., Sun, D., Bloemendal, J. and Zhu, Z.: Temporal and spatial variability of the oxygen
521 isotopic composition of massive corals from the South China Sea: Influence of the Asian
522 monsoon, *Palaeogeogr. Palaeoclimatol. Palaeoecol.*, 240(3–4), 630–648,
523 <https://doi.org/10.1016/j.palaeo.2006.03.012>, 2006.
- 524 Sun, D., Gagan, M. K., Cheng, H., Scott-Gagan, H., Dykoski, C. A., Edwards, R. L. and Su, R.:
525 Seasonal and interannual variability of the Mid-Holocene East Asian monsoon in coral $\delta^{18}\text{O}$
526 records from the South China Sea, *Earth Planet. Sci. Lett.*, 237(1–2), 69–84,
527 <https://doi.org/10.1016/j.epsl.2005.06.022>, 2005.
- 528 Toth, L. T. and Aronson, R. B.: The 4.2 ka event, ENSO, and coral reef development, *Clim. Past*, 15,
529 105–119, <https://doi.org/10.5194/cp-15-105-2019>, 2019.
- 530 Tudhope, A. W., Chilcott, C. P., McCulloch, M. T., Cook, E. R. and coauthors: Variability in the El
531 Niño-Southern Oscillation through a glacial-interglacial cycle, *Science.*, 291, 1511–1517,
532 2001.



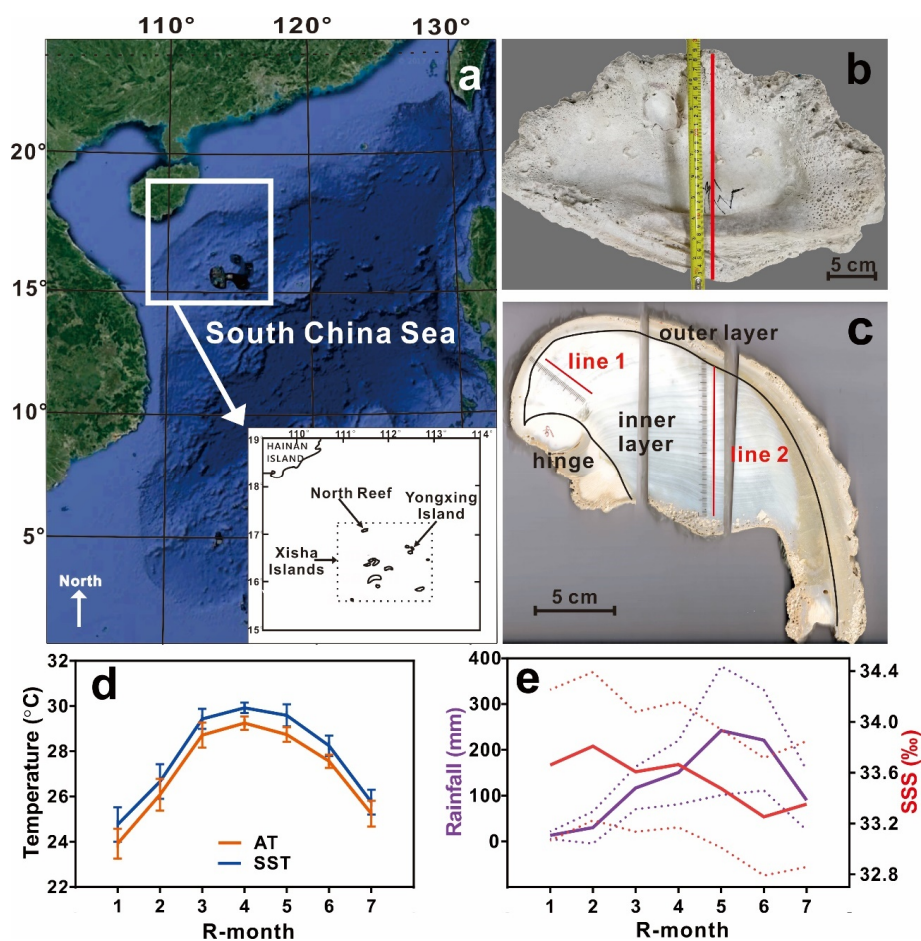
- 533 Wanamaker, A. D., Kreutz, K. J., Schöne, B. R. and Introne, D. S.: Gulf of Maine shells reveal
534 changes in seawater temperature seasonality during the Medieval Climate Anomaly and the
535 Little Ice Age, *Palaeogeogr. Palaeoclimatol. Palaeoecol.*, 302(1), 43–51,
536 <https://doi.org/10.1016/j.palaeo.2010.06.005>, 2011.
- 537 Wang, J., Wang, S., Zhang, Q., Li, Y., Wang, J. and Zhang, J.: Characteristics of drought
538 disaster-causing factor anomalies in southwestern and southern China against the
539 background of global warming, *Polish J. Environ. Stud.*, 24(5), 2241–2251,
540 <https://doi.org/10.15244/pjoes/58764>, 2015.
- 541 Watanabe, T., Oba, T. and Dee, V.: Daily reconstruction of water temperature from oxygen
542 isotopic ratios of a modern *Tridacna* shell using a freezing microtome sampling technique
543 was recorded monthly to seasonal sea surface to reconstruct using Jones maturity of
544 *Tridacna maxima* resolution f, *J. Geophys. Res.*, 104(C9), 20667–20674, 1999.
- 545 Watanabe, T., Suzuki, A., Kawahata, H., Kan, H. and Ogawa, S.: A 60-year isotopic record from a
546 mid-Holocene fossil giant clam (*Tridacna gigas*) in the Ryukyu Islands: Physiological and
547 paleoclimatic implications, *Palaeogeogr. Palaeoclimatol. Palaeoecol.*, 212(3–4), 343–354,
548 <https://doi.org/10.1016/j.palaeo.2004.07.001>, 2004.
- 549 Wei, G., Deng, W., Yu, K., Li, X. H., Sun, W. and Zhao, J. X.: Sea surface temperature records in
550 the northern South China Sea from mid-Holocene coral Sr/Ca ratios, *Paleoceanography*,
551 22(3), 1–13, <https://doi.org/10.1029/2006PA001270>, 2007.
- 552 Welsh, K., Elliot, M., Tudhope, A., Ayling, B. and Chappell, J.: Giant bivalves (*Tridacna gigas*) as
553 recorders of ENSO variability, *Earth Planet. Sci. Lett.*, 307(3–4), 266–270,
554 <https://doi.org/10.1016/j.epsl.2011.05.032>, 2011.
- 555 Woodroffe, C. D., Beech, M. R. and Gagan, M. K.: Mid-late Holocene El Niño variability in the
556 equatorial Pacific from coral microatolls, *Geophys. Res. Lett.*, 30(7), 1–4,
557 <https://doi.org/10.1029/2002GL015868>, 2003.
- 558 Yamanashi, J., Takayanagi, H., Isaji, A., Asami, R. and Iryu, Y.: Carbon and oxygen isotope
559 records from *Tridacna derasa* shells: Toward establishing a reliable proxy for sea surface
560 environments, *PLoS One*, 11(6), <https://doi.org/10.1371/journal.pone.0157659>, 2016.
- 561 Yan, H. and Sun, L.: Relationship between ENSO events and regional climate anomalies around
562 the Xisha Islands during the last 50 years, *J. Trop. Oceanogr.*, 29(5), 29–35,
563 <https://doi.org/10.1007/s13131-014-0399-4>, 2010.
- 564 Yan, H., Shao, D., Wang, Y. and Sun, L.: Sr/Ca profile of long-lived *Tridacna gigas* bivalves from
565 South China Sea: A new high-resolution SST proxy, *Geochim. Cosmochim. Acta*, 112, 52–
566 65, <https://doi.org/10.1016/j.gca.2013.03.007>, 2013.
- 567 Yan, H., Wang, Y. and Sun, L.: High resolution oxygen isotope and grayscale records of a
568 medieval fossil giant clam (*Tridacna gigas*) in the South China Sea: Physiological and
569 paleoclimatic implications, *Acta Oceanol. Sin.*, 33(8), 18–25,
570 <https://doi.org/10.1007/s13131-014-0399-4>, 2014.
- 571 Yan, H., Liu, C., Zhang, W., Li, M., Zheng, X., Wei, G., Xie, L., Deng, W. and Sun, L.: ENSO
572 variability around 2000 years ago recorded by *Tridacna gigas* $\delta^{18}\text{O}$ from the South China
573 Sea, *Quat. Int.*, 452, 148–154, <https://doi.org/10.1016/j.quaint.2016.05.011>, 2017.
- 574 Yang, Y., Xiang, R., Liu, J. and Tang, L.: Inconsistent sea surface temperature and salinity
575 changing trend in the northern South China Sea since 7.0 ka BP, *J. Asian Earth Sci.*, 171,
576 178–186, <https://doi.org/10.1016/j.jseas.2018.05.033>, 2019.



- 577 Yu, J., Qi, M., Sun, Q. and Tao, L.: Statistical characteristics of summer extreme rainfall over
578 eastern China and its relation with El Niño, *J. Nanjing Inst. Meteorol.*, 41(1), 77–84,
579 available from: <http://lib.cqvip.com/qk/91555A/201801/7000486505.html>, 2018a.
- 580 Yu, K. F., Zhao, J. X., Wei, G. J., Cheng, X. R. and Wang, P. X.: Mid-late Holocene monsoon
581 climate retrieved from seasonal Sr/Ca and $\delta^{18}\text{O}$ records of *Porites lutea* corals at Leizhou
582 Peninsula, northern coast of South China Sea, *Glob. Planet. Change*, 47(2-4 SPEC. ISS.),
583 301–316, <https://doi.org/10.1016/j.gloplacha.2004.10.018>, 2005.
- 584 Yu, R., Zhai, P. and Chen, Y.: Facing climate change-related extreme events in megacities of China
585 in the context of 1.5 °C global warming, *Curr. Opin. Environ. Sustain.*, 30, 75–81,
586 <https://doi.org/10.1016/j.cosust.2018.03.008>, 2018b.
- 587 Yu, X., Wang, Z., Zhang, H. and Zhao, S.: Impacts of different types and intensities of El Niño
588 events on winter aerosols over China, *Sci. Total Environ.*, 655, 766–780,
589 <https://doi.org/10.1016/j.scitotenv.2018.11.090>, 2019.
- 590 Zhang, H., Cheng, H., Cai, Y., Spötl, C., Kathayat, G. and Sinha, A.: Hydroclimatic variations in
591 southeastern China during the 4.2 ka event reflected by stalagmite records, *Clim. Past*,
592 14(11), 1805–1817, <https://doi.org/10.5194/cp-14-1805-2018>, 2018.
- 593
594
595
596
597
598
599
600
601
602
603
604
605
606
607
608
609
610
611
612
613
614
615
616
617
618
619



620 **Figures**



621

622 **Figure 1.** Maps of the South China Sea, with the location of the study area in the Xisha Islands (a).

623 Photo of *Tridacna* A5, and a slice was cut along the maximum growth axis (red line) from the

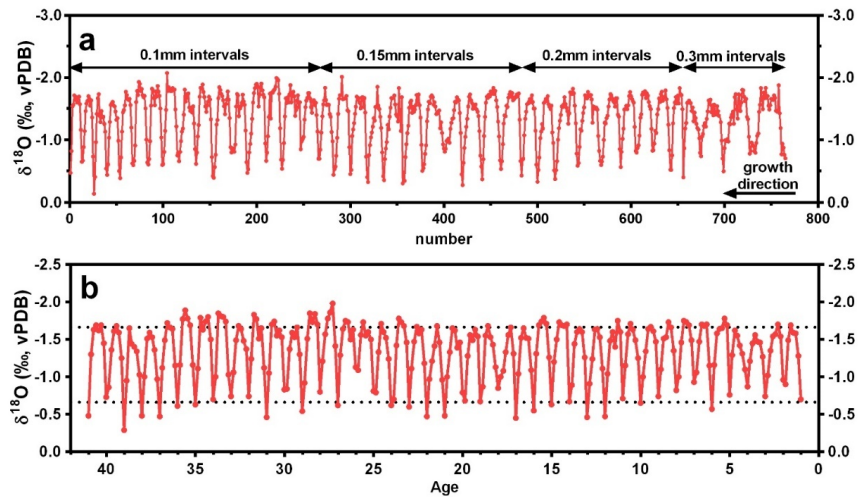
624 umbo to the ventral margin (b). Different parts can be seen clearly (hinge, inner layer, and outer

625 layer) (c), the red lines are the sampling lines for $\delta^{18}\text{O}$ analysis. Meteorological observations in the

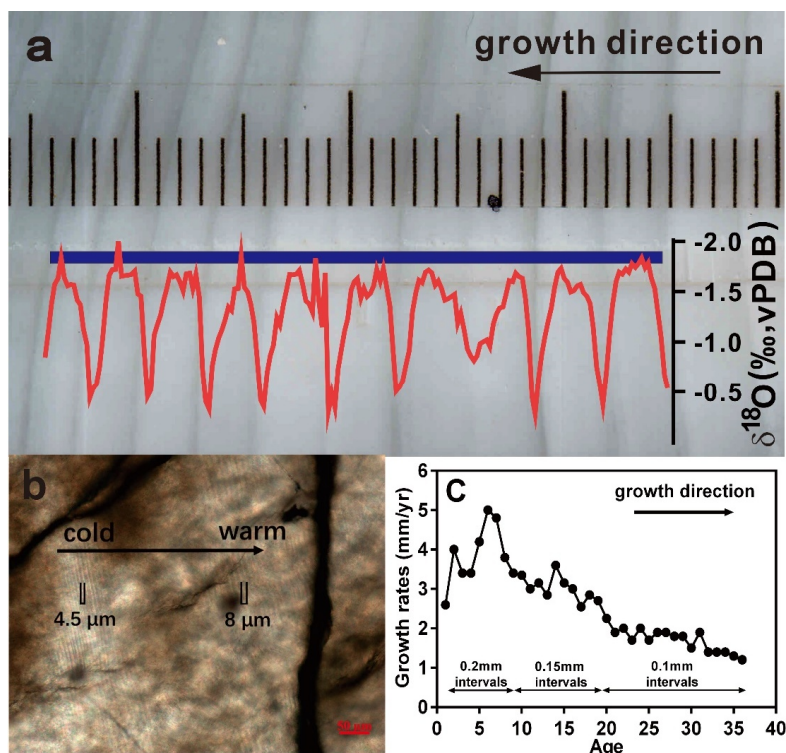
626 Xisha Islands from 1994 to 2005: R-monthly average air temperature (AT) and sea surface

627 temperature (SST) (d); R-monthly average rainfall and sea surface salinity (SSS) with standard

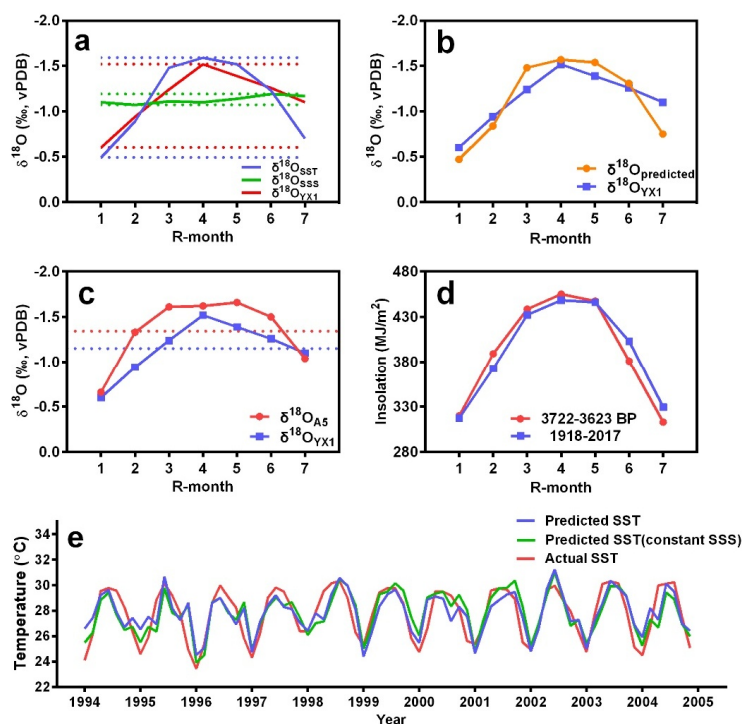
628 deviation (1σ) (e).



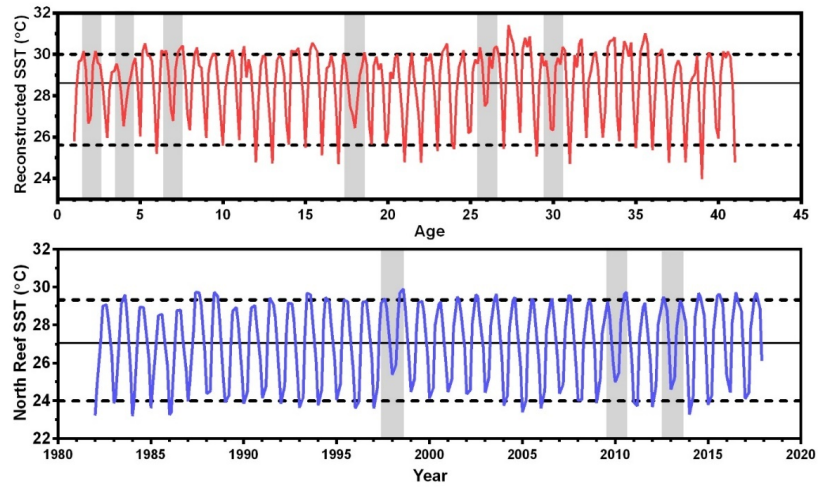
629
630 **Figure 2.** The $\delta^{18}\text{O}$ profiles of A5 (a). The $\delta^{18}\text{O}_{\text{A5}}$ series with chronology time-scale after
631 rehandling data, and the dotted lines indicate the average of annual maximum and minimum (b).



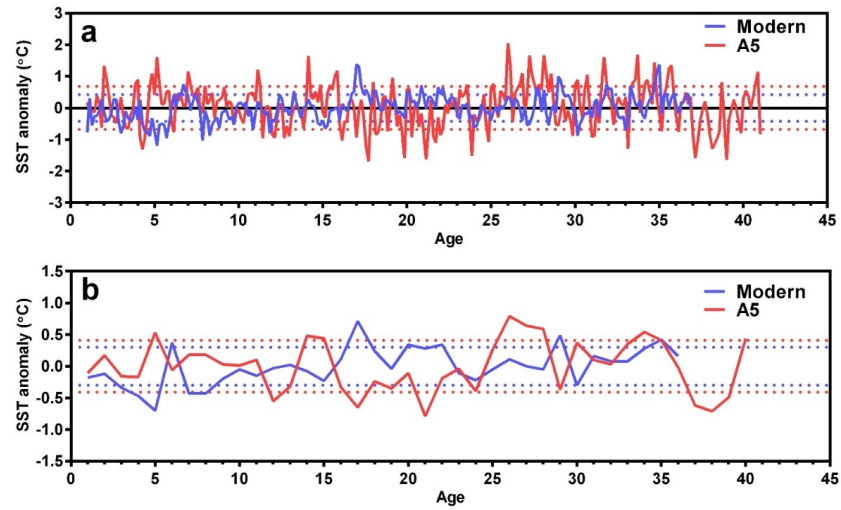
632
633 **Figure 3.** Amplitude of dark/light couples, consistent with $\delta^{18}\text{O}_{\text{A5}}$ profiles. Dark and light
634 increments correspond to high $\delta^{18}\text{O}$ (cold seasons) and low $\delta^{18}\text{O}$ (warm seasons). Blue line
635 represents the sampling line (a). Under the microscope, daily increments grow slower in cold
636 seasons, but faster in warm seasons (b). Growth rates (line 2) in fossil *Tridacna* A5 (c).



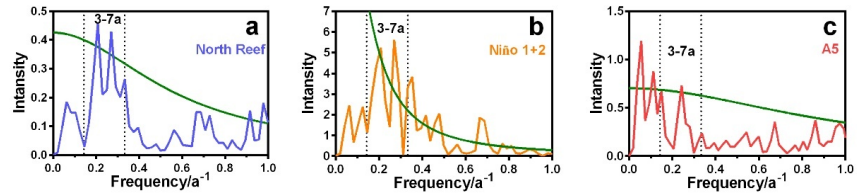
637
 638 **Figure 4.** Predicted r-monthly $\delta^{18}\text{O}$ profiles under constant SSS (blue line) and constant SST
 639 (green line) conditions, and $\delta^{18}\text{O}$ of YX1 (red line). Dotted lines represent the maximum and
 640 minimum of the r-monthly $\delta^{18}\text{O}$ profiles (a). R-Monthly average $\delta^{18}\text{O}_{\text{YX1}}$ and $\delta^{18}\text{O}_{\text{predicted}}$ (b).
 641 R-monthly average $\delta^{18}\text{O}_{\text{YX1}}$ and $\delta^{18}\text{O}_{\text{A5}}$, and the dotted lines represent mean values (c). Different
 642 insolation in 3700 years ago and in the recent 100 years (d). Different SST profiles: predicted SST
 643 with varied SSS (blue line), constant mean SSS (green line), and actual SST (red line) (e).



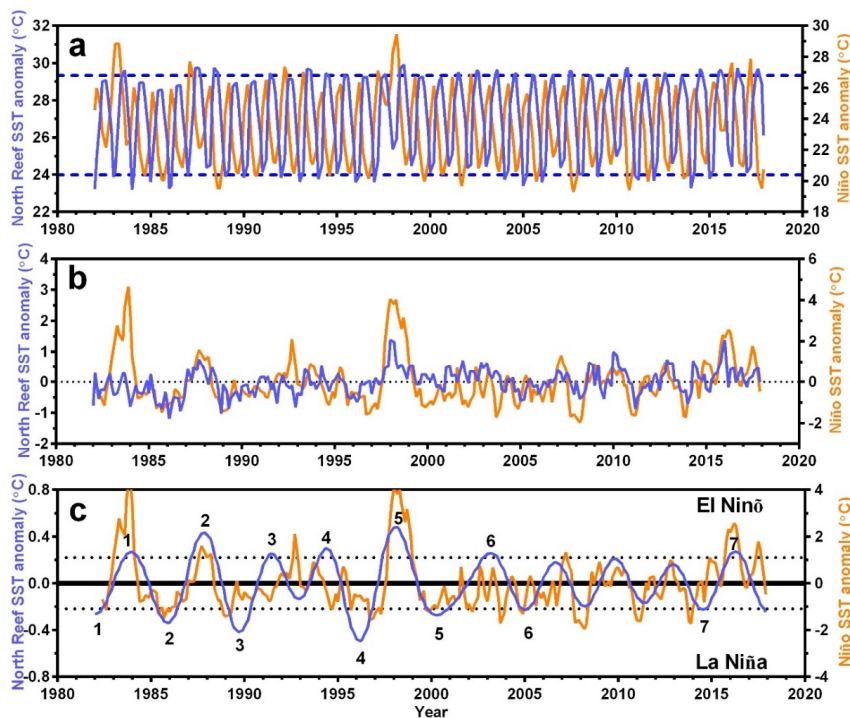
644
645 **Figure 5.** Reconstructed SST around 3700 years ago (red), compared with the North Reef SST
646 from 1982 to 2017 (blue). Dotted lines represent the average maximum and minimum SST. Gray
647 field represents the extreme winter El Niño events.



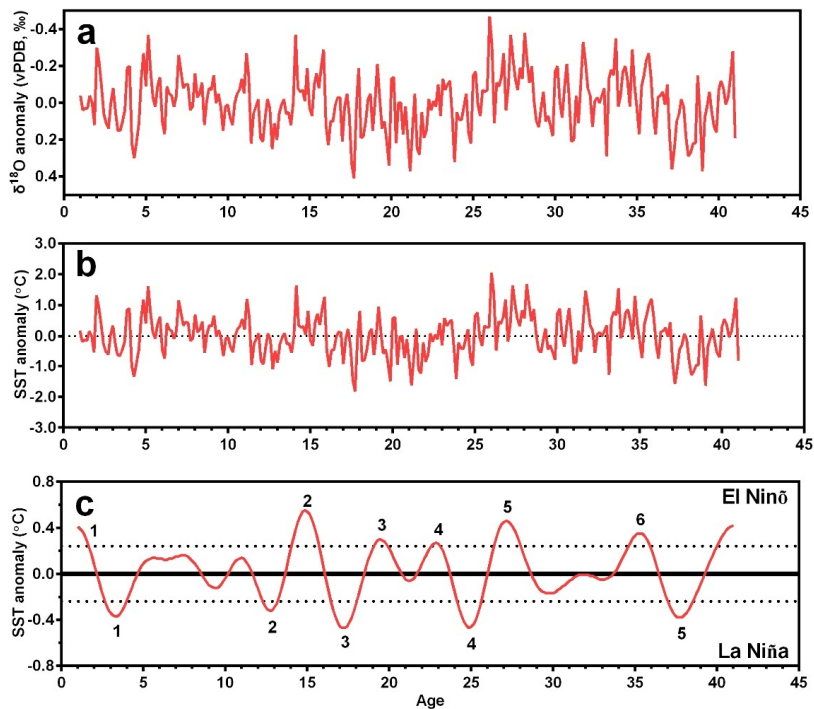
648
649 **Figure 6.** SST anomalies of modern instrument data and reconstructed SST anomalies of *Tridacna*
650 *A5* under *r*-monthly (a) and *r*-annual (b) resolution. Dotted lines represent one standard deviation
651 (1σ) of SST anomalies.



652
653
654 **Figure 7.** Spectral analysis of the North Reef SST anomalies (a), Niño 1 + 2 SST anomalies (b),
655 and reconstructed SST anomalies according to $\delta^{18}\text{O}_{A5}$ (c). Green lines indicate significant lines at
656 90 % confidence level, and the area between two dotted lines represents the frequency from 3 to 7
657 years.



658
659 **Figure 8.** Relationship between ENSO activity and the North Reef SST: The North Reef SST
660 (blue line) compared with Niño 1 + 2 SST (yellow line), a clear time lag exists (a). SST anomalies
661 of two areas, and the lag is removed by forwarding the North Reef SST anomalies for 3 r-months
662 (b). The North Reef SST anomalies performed with 3-7 years bandpass filter, consistent with Niño
663 1 + 2 SST anomalies, and the dash lines show the calculated threshold limits (1σ) for El Niño and
664 La Niña events in the North Reef (c). El Niño and La Niña events are represented by positive and
665 negative SST anomalies values, respectively.



666
667 **Figure 9.** ENSO activity reconstructed by fossil *Tridacna* 3700 years ago: $\delta^{18}\text{O}$ anomalies of
668 fossil *Tridacna* A5 (a). The North Reef SST anomalies calculated by $\delta^{18}\text{O}$ anomalies (b), based on
669 modern *Tridacna* $\delta^{18}\text{O}$ -SST equation ($1\text{‰ } \delta^{18}\text{O}_{\text{shell}} \approx 4.41^\circ\text{C}$ SST). ENSO activity according to
670 the North Reef SST anomalies after 3-7 years bandpass filtering, and the dash lines show the
671 calculated threshold limits (1σ) for El Niño and La Niña events (c).